Pergamon

Journal of Structural Geology, Vol. 17, No. 3, pp. 423 to 434, 1995

0191-8141/95 $9.50+0.00

0191-8141(94)00058-1

Relation between vein length and aperture

JAN M. VERMILYE and CHRISTOPHER H. SCHOLZ

Lamont-Doherty Earth Observatory and Department of Geological Sciences, Columbia University, Palisades, NY 10964-0190, U.S.A.

(*Received* 4 *October* 1993; *accepted in revised form* 21 *April* 1994)

Abstract—Veins formed in a variety of rock types and tectonic environments were measured at seven field locations to determine a general scaling relationship between the length and opening displacement (aperture). For these naturally formed extension fractures displacement-length profiles for both single- and multiple-segment veins display centrally located maxima and gently tapered displacement gradients at the tips. This geometry is consistent with elastic-plastic crack growth models, which also predict linear scaling between length and displacement. The geometry is used to estimate stresses of formation for the veins. Length-maximum displacement plots for single-segment fractures show data clustered along linear trends. Similar plots for multiple-segment fractures show greater scatter and are marginally better fit by a square root function than by a line. The geometries of multiple-segment veins are consistent with elastic models for crack-tip stress interactions. Aspect ratios for single-segment fracture sets vary between 1×10^{-3} and 8×10^{-3}, consistent with tensional fracture strengths roughly an order of magnitude lower than compressive shear strengths implied by shear displacement-length ratios recorded for faults, which are about 10^{-2}.

INTRODUCTION

Naturally occurring extension fractures are among the most common structural features in the earth's crust (Broek 1974, Pollard & Aydin 1988) and as such, an understanding of their detailed geometric characteristics is of practical as well as theoretical importance. Fracture studies have practical applications in hydrology, mining and engineering since fractures significantly influence fluid storage and transport, mineral deposition, and the strength of the rocks in which they form. Field observations on the geometry of fractures constrain theoretical models of fracture initiation and propagation.

Elastic crack theory is the conventional method used for describing the propagation and resulting displacements of fractures in brittle rock (Broek 1974, Lawn & Wilshaw 1975). The required idealization of rock as a homogeneous, isotropic, linear elastic material has proved satisfactory for explaining many, but not all aspects of fracture behavior (e.g. Delaney & Pollard 1981, Pollard & Segall 1987, Bürgmann *et al.* 1994). Displacement profiles for idealized elastic cracks are elliptical with maximum displacement gradients at the crack tips. This elliptical shape results in a stress singularity at the crack tip, which is unrealistic for earth materials which are not perfectly elastic but exhibit finite strength. Elastic theory predicts that opening displacement for mode I fractures scales linearly with fracture length (Pollard & Segall 1987).

Elastic-plastic fracture mechanics models utilize elastic theory to describe deformation of the main body of a crack while addressing the inability of purely elastic models to describe deformation in the crack tip region. Dugdale's elastic-plastic model (1960) proposed a cohesion zone of inelastic deformation at the tip of a tensile crack. Goodier & Field (1963) used Dugdale's model to describe displacements along the length of the crack. These displacements produce tapered profiles as well as predicting linear scaling between maximum displacement and fracture length. The constant of proportionality is dependent on the ratio between yield strength and shear modulus for the fractured material (Cowie & Scholz 1992). The aspect ratio is defined as the maximum aperture (displacement measured perpendicular to the fracture wall) divided by the fracture length and as such is equivalent to the above mentioned proportionality constant.

The displacement geometry of extension fractures, as they exist in the subsurface, may be affected by post-formation alterations in aperture. Measurement of fractures that are mineralized at depth (veins) reduces this problem. Veins with geometry most likely to be representative of the geometry of the original fractures were chosen for analysis in this study. We selected mode I extension veins that show no field evidence of shear displacement, subsequent deformation or incremental growth textures, any of which might indicate alteration of the original aperture.

The apertures measured are lower bounds for each fracture, since some amount of closure may have occurred prior to mineralization. We presume that changes in the remote stress or fluid pressure that might cause such closure similarly affect all fractures at a given locality and with a common orientation. Therefore, it is reasonable to assume that the scaling between length and aperture is maintained throughout each vein set studied.

While the smallest fractures measured consist of single, isolated segments, longer fractures are commonly composed of a number of closely spaced, subparallel segments. These segments are in some cases observed to be connected below the surface of obser-

vation, but in general, this information is not available. For single-segment fractures measurement of length and aperture is straightforward. The length measurement for multiple-segment fractures may be ambiguous when it is unclear whether the segments should be considered as isolated fractures or as parts of a larger fracture. In this study, criteria are developed for determining which groups of segments constitute single features for use in the measurement of fracture length.

The purpose of this paper is to describe the geometry of extensional fractures, based on new field observations. We suggest that carefully selected veins display geometries representative of fractures at the depth of formation and that these geometries constrain models and physical properties related to rock fracture. The observed geometries are discussed in terms of an elastic-plastic fracture mechanics model for single-segment fractures. Multiple-segment fracture geometries are discussed in terms of a model that includes the elastic interactions between component segments.

OBSERVATIONS

Seven field locations were selected, representing a range of rock types and tectonic environments. At each location only one fracture set, with a consistent strike, dip and mineral filling, was selected for measurement. This was done in order to limit data to fractures formed within a single tectonic environment. To measure fractures over the greatest possible range of lengths, planar exposures were selected with areal dimensions much greater than the longest fractures present. A total of 664 fractures were measured. Descriptions of field locations are included in the Appendix.

The orientations of veins described in this study are consistent with formation as vertical extension fractures, which in many cases can be shown to result from regional stresses (see Appendix). Their basic geometry can be described with length, width and aperture measurements. The vein length and width are defined as the maximum dimensions measured parallel and normal to the earth's surface (at the time of formation). Aperture is defined as the opening displacement measured normal to the vein walls. For most veins data are available only as vein traces (i.e. the intersection between the vein and the outcrop surface). The trace geometries of selected vein sets were recorded in the field with detailed measurements of traces. A tape measure was laid parallel to and along each vein trace and apertures were measured with dial calipers at regular intervals along the length. The calipers allow measurement of apertures as small as 0.1 ± 0.05 mm. Measurements of single-segment fractures were made on isolated veins to eliminate the effects of stress perturbations caused by neighboring fractures. For multiple-segment fractures the perpendicular offset between adjacent fracture segments, as well as the overlap measured parallel to the strike of the segments were recorded.

Since structures indicating alterations of aperture are difficult to detect in the field we collected samples for microscopic analysis. Thin-sections made from vein samples were examined in ordinary and polarized light and with a M.A.A.S. Nuclide Cathodoluminescope. For five of the seven localities the microscopic analysis supported the field observations.

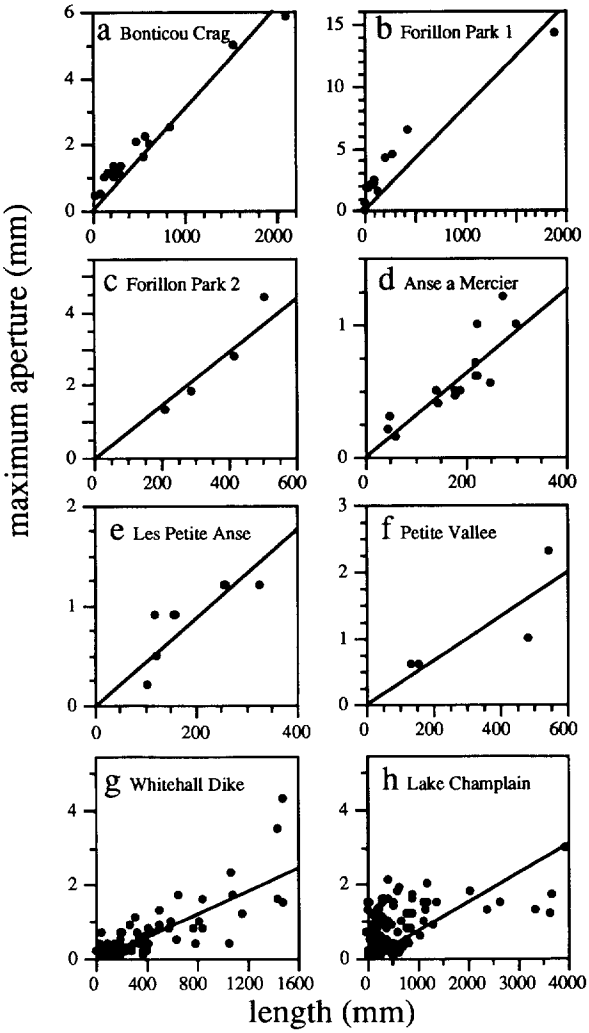

Fig. 1. Length-maximum aperture plots for single-segment fractures (for this and the following figures, A = maximum aperture, L = length, R^2 = correlation coefficient). (a) Bonticou Crag ($A = 3.1 \times 10^{-3}L$, $R^2 = 0.96$). (b) Outcrop 1, Forillon Park, Gaspe Peninsula ($A = 8.2 \times 10^{-3}L$, $R^2 = 0.86$). (c) Outcrop 2, Forillon Park, Gaspe Peninsula ($A = 7.3 \times 10^{-3}L$, $R^2 = 0.94$). (d) Anse a Mercier, Gaspe Peninsula ($A=3.1 \times 10^{-3}L$, $R^2 = 0.73$). (e) Les Petite Anse, Gaspe Peninsula ($A = 4.4 \times 10^{-3}L$, $R^2 = 0.66$). (f) Petite Vallee, Gaspe Peninsula ($A = 3.3 \times 10^{-3}L$, $R^2 = 0.68$). (g) Whitehall Dike ($A = 1.5 \times 10^{-3}L$, $R^2 = 0.66$). (h) Lake Champlain ($A = 7.7 \times 10^{-4}L$, $R^2 = 0.24$).

The length and maximum aperture for single-segment fractures are shown in Fig. 1, with data from Bonticou Crag, Whitehall Dike, Lake Champlain and five locations on the Gaspe Peninsula. These veins were assumed to represent single-event, undeformed fractures based on field observations of blocky crystal growth of the vein-filling material. Microscopic examination of vein samples confirmed that conclusion for all locations except Whitehall Dike. In the Whitehall veins a subtle, linear texture parallel to the vein walls is observed in the calcite and chlorite vein-filling material. This may result from crack-seal growth (Ramsay 1980) or shear defor-

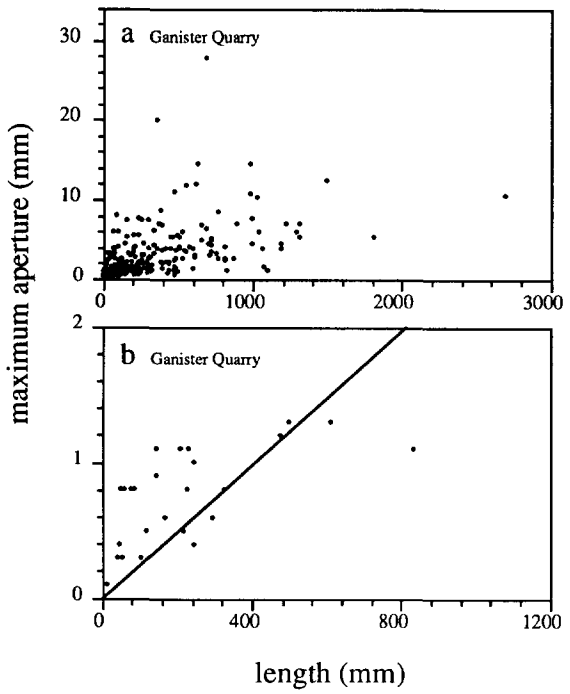

Fig. 2. Length-maximum aperture plots for veins from Ganister Quarry. (a) All veins measured, including sheared and multi-increment veins. (b) Ganister Quarry, undeformed, single-event fractures ($A = 2.5 \times 10^{-3}L$, $R^2 = 0.28$).

mation, either of which might alter the aspect ratios for this data set.

At Ganister Quarry data were collected for all veins intersecting an 80 m^2 exposure of a bedding plane (Fig. 2a). Some veins showed field evidence of shear deformation and/or crack-seal morphology, indicating several incremental growth events. Therefore, a subset of undeformed, single-event fractures was selected, by visual inspection, from the larger data set (Fig. 2b). Microscopic examination of samples from this subset shows blocky calcite grains, consistent with a single-event formation for these fractures.

The last two field locations have spectacular planar exposures and contain the longest fractures measured. Culpeper Quarry contains fractures cutting a layered siltstone lithology. The Florence Lake fractures cut a massive granodiorite body. These large exposed areas make a comprehensive comparison of single- and multiple-segment fractures possible for both locations. Longer veins are composed of closely spaced en échelon segments, showing both left- and right-stepping sense between segments in a single vein system. In small exposures perpendicular to the major outcrop surfaces, some separate segments can be seen to be connected at depth.

In Culpeper Quarry 23 fractures 65 mm–13.2 m long were measured (Fig. 3a). The number of segments ranged from 1 to 71 per vein. A 13 m long, 71-segment vein was selected for a study of segmentation. Aperture measurements were made every 5 mm along this fracture's length. This procedure was carried out in order to record the individual segment shapes and the relationships between adjacent segments. At Florence Lake 42 veins were measured, ranging in length from 23 mm to 23.7 m (Fig. 3b). The number of segments per vein ranges between 1 and 40, with longer veins generally containing more segments. Thin section analysis shows randomly oriented chlorite and epidote grains in veins from Florence Lake and equant calcite grains in the single-segment veins from Culpeper Quarry. Microscopic crack-seal structure was observed in a multi-segment vein from Culpeper Quarry indicating repeated cracking and sealing events. Inclusion of undetected crack-seal veins in this data set may tend to increase aspect ratios.

DATA ANALYSIS

The data collected exhibit a positive correlation between length and aperture. In Fig. 1 through Fig. 3 lines through the data are least square fits with a specified zero intercept, calculated using the Levinberg–Marquardt method (Press *et al.* 1986). The parameters for these fits are indicated on the figures or in the captions. The proportionality constants range from 2.1×10^{-4} to 8.2×10^{-3}, while correlation coefficients range from very good to very weak.

General problems

The maximum aperture-length plots display many of the statistical problems encountered in analysis of this type of field data (Figs. 1 and 2). Considerable scatter results from geologic irregularity (i.e. local variations in rock properties or stress field) and from the measurement techniques used in data collection. Most plots show clustering of data near the origin. This clustering reflects the greater frequency of smaller fractures and is a consequence of the power-law size distribution typically observed for fracture populations (Segall & Pollard 1983, Barton & Larsen 1985, Scholz & Cowie 1990). The data loses resolution at the lower end of the range owing to the inability to measure apertures smaller than 0.05 mm with the dial calipers. This results in a bias in the distribution of variance near the origin, where the bulk of the data is located. These non-normal distributions render standard linear regression techniques for obtaining correlation coefficients questionable for many of the data sets.

Scatter in the plots also results from variation in the orientation of the observed fracture traces with respect to the actual shape of the three dimensional fractures. Scatter in the data increases for multiple-segment fractures. We attribute some of this scatter to variability in the number and connectedness of the fracture segments, as will be discussed later. Scatter may also result from inclusion of undetected crack-seal fractures in the data sets.

Fracture segmentation

The smallest veins measured as each location are single, isolated features. Longer fractures are composed

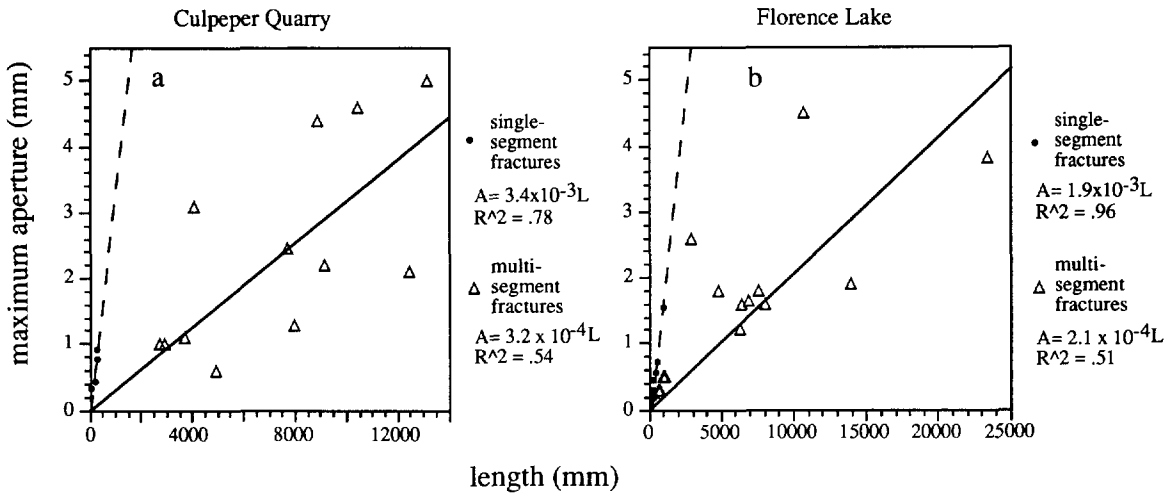

Fig. 3. Length-maximum aperture plots for fractures from Culpeper Quarry (a) and Florence Lake (b). Single-segment fractures from both locations show larger aspect ratios and better correlation between length and aperture than multiple-segment fractures.

of closely spaced, sub-parallel segments. The segments display varying degrees of connectedness. Some segments are not visibly connected while others are attached to adjacent segments by smaller connecting veins. For some fractures the connection is complete, with a kink in the orientation of the vein walls revealing the location of the point of coalescence (Fig. 4). Vein traces that are non-connected or partially connected on planar outcrop surfaces have been observed to be well connected at depth when three-dimensional outcrop exposures are available. When three-dimensional information is not available, displacement-length profiles can provide insight on the connectedness of the segments. Figure 5(a) shows the displacement-length profile for a single-segment fracture. The profile displays a roughly centrally located maximum, with tapered displacement gradients at the tips. The multi-segment fracture in Fig. 5(b) is composed of 11 closely spaced, sub-parallel, yet physically non-connected segments. The 11 segments as a whole display a shape similar to that of the single-segment fracture. The individual segments do not appear to be independent, but accommodate displacement as a collective unit, in much the same way as the single-segment feature. It is on this basis that we treat such multi-segment veins as a single unit when making length measurements.

Detailed measurement of a 71-segment fracture from Culpeper Quarry reveals a self-similarity of segment shapes in a hierarchy of vein segmentation. The displacement-length profile is shown in Fig. 6(a). The overall shape indicates that the segments are acting as a unit to accommodate deformation, as in Fig. 5(b). The profile is not uniformly smooth, but is marked by discontinuities or cusps in the magnitude of the aperture. These discontinuities mark points of displacement deficit along the fracture profile.

The map view in Fig. 6(b) shows the small relative magnitude of perpendicular offset with respect to frac-

Fig. 4. Sketch showing adjacent segments with varying degrees of connectedness. (a) Non-connected segments. (b) Partially connected segments. (c) Well connected segments. Note large vertical exaggeration.

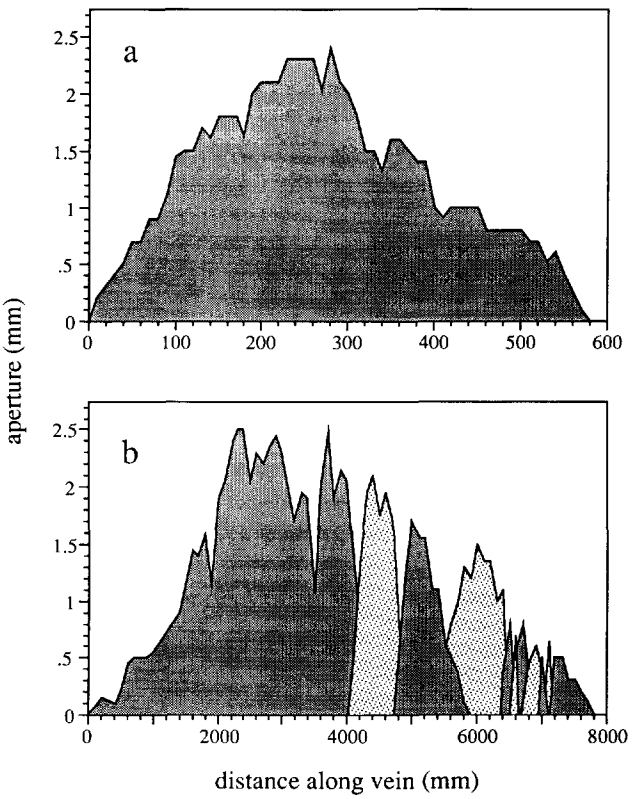

Fig. 5. Single- and multiple-segment veins display similar shapes for displacement-length profiles. (a) A single-segment fracture. (b) An 11-segment fracture. Segments are shown with grey tone and stipples. Note the difference in scales.

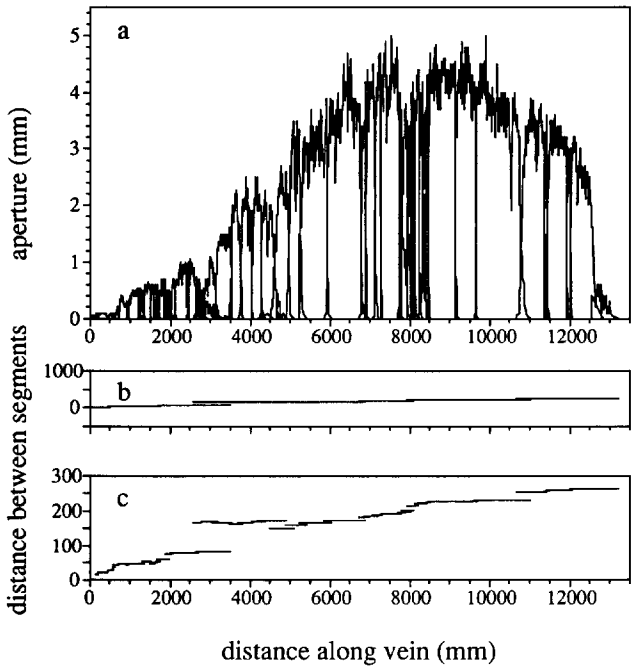

Fig. 6. (a) Displacement-length profile for a 71-segment fracture from Culpeper Quarry. (b) Map view of the fracture segments. (c) Map view with vertical scale expanded by an order of magnitude.

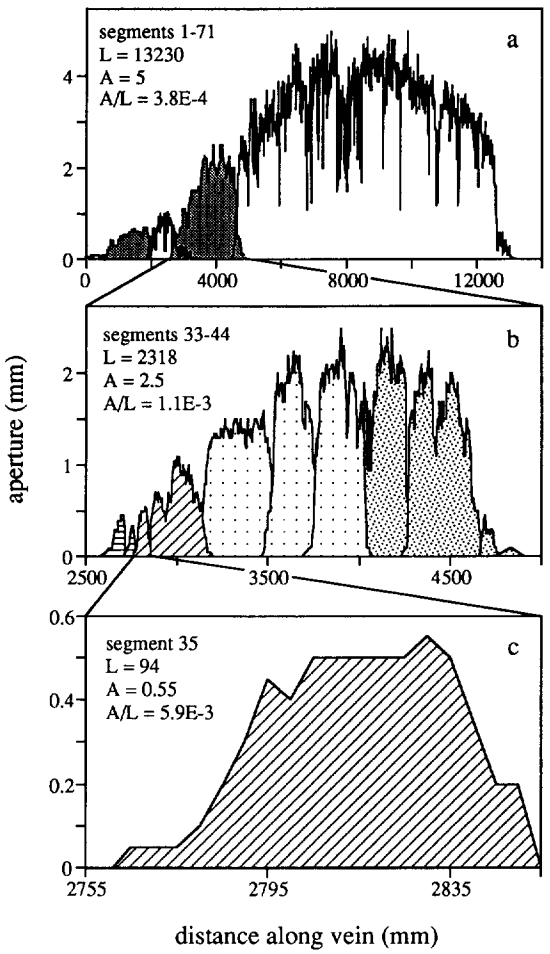

Fig. 7. Aperture-length profiles for a 71-segment vein from Culpeper Quarry. (a) The total fracture is divided into six subunits defined by discontinuities. Note, the first two subunits are less than 500 mm in length and therefore difficult to discern at this scale. (b) A first-order subunit from (a). Two second-order subunits are shown, one with stipples and one with lines. Third-order subunits are shown by variations in the line and stipple patterns. (c) A fourth-order subunit.

ture length, supporting the interpretation that the 71 segments act as a single unit. Expanding the vertical scale by an order of magnitude (Fig. 6c) reveals details of segmentation not discernable when the vertical and horizontal scales are equal. The perpendicular offset between adjacent segments is considerably larger for some pairs of segments. These pronounced perpendicular offsets correlate with larger overlaps measured parallel to the segment length. These larger offsets and overlaps correlate in turn to the larger displacement deficits noted above. The larger offsets and displacement deficits are used to define somewhat independent subunits within the fracture (Fig. 7). The first-order subunits display tapered profiles (e.g. Fig. 7b) similar to the profile of the fracture as a whole. Each of the first-order subunits shown in Fig. 7(a) can be divided into second-order subunits using the same criteria that were used to define the first-order subunits (Fig. 7b). This process can be repeated to define third- and fourth-order subunits. The fourth-order subunits are the original 71 segments measured in the field (Fig. 7c).

Two trends exist in the maximum aperture-length relationships (Fig. 8). First, the average aspect ratio for subunits steadily increases from the larger, first-order subunits to the smaller fourth-order subunits. The whole 71-segment fracture and its first-through third-order subunits have aspect ratios smaller than those of isolated single-segment fractures in the same outcrop (3.4×10^{-3}, Fig. 3a). The fourth-order subunits, the individual segments, have on average higher aspect ratios than isolated fractures. Second, the maximum aperture and length for higher order subunits are less well correlated than for lower order subunits. Length and maximum aperture of fourth-order subunits are practically uncorrelated. We interpret this decreasing correlation as an indication that these subunits are not acting as independent units. Their shapes, represented by their aspect ratios, are dependent on their location with respect to adjacent subunits, as can be seen in the shape of the fracture as a whole. While no evidence for incremental growth was observed in this multi-segment vein, the possibility remains that undetected crack-seal growth may contribute to the observed scatter in aspect ratios.

Aspect ratios for single- and multiple-segment fractures

The aspect ratio for individual fractures is defined as the maximum aperture divided by the fracture length. We have calculated an average aspect ratio for each data set by fitting a line to the data. The line is constrained to pass through the origin, reflecting the constraint that a fracture of zero length must also have a zero aperture. Due to the wide scatter and statistical problems inherent in the data, curves fit to the data are often poorly constrained. Average aspect ratios for the data sets containing single-segment fractures are shown in Table 1, where the data are grouped according to lithology. For the higher quality data sets ($R^2 > 6$) there is an

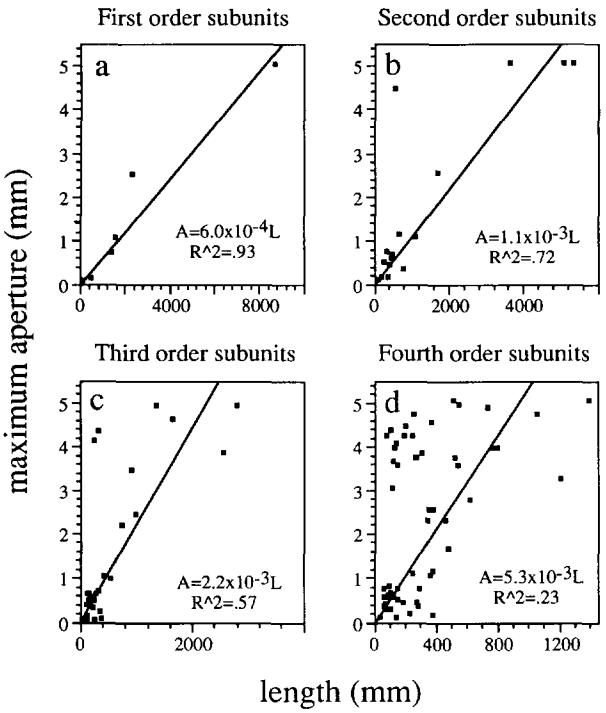

Fig. 8. Length-maximum aperture plots for subunits making up a multiple-segment vein from Culpeper Quarry. (a) First-order subunits. (b) Second-order subunits. (c) Third-order subunits. (d) Fourth-order subunits.

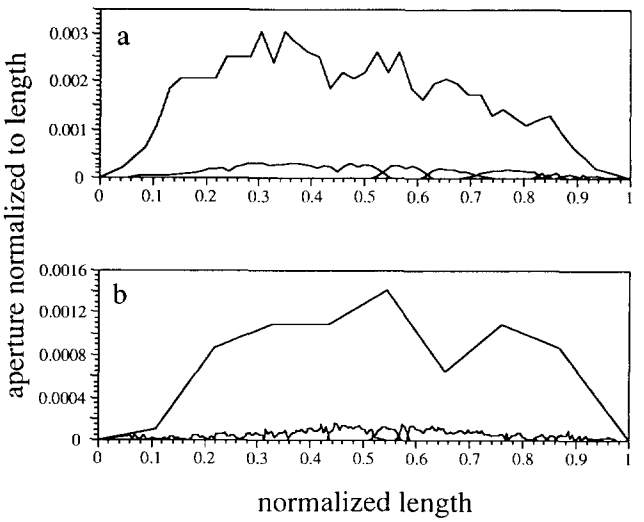

Fig. 9. The lengths of single- and multi-segment fractures are normalized and the apertures are normalized to the length in order to preserve the relative aspect ratios. (a) A 230 mm long single-segment fracture and a 7.8 m long 11-segment fracture from Culpeper Quarry. (b) A 460 mm long single-segment fracture and a 23.5 m long 26-segment fracture from Florence Lake.

increase in aspect ratio from igneous rocks to quartz-rich sedimentary rocks to limestone. This increase in aspect ratio may reflect an increase in ductility (e.g. Bürgmann *et al.* 1994). Increased ductility is consistent with higher levels of pressure solution activity observed in these rock types.

While the linear curves fit to the data are often poorly constrained due to scatter inherent in the data sets, the fit is not improved, and in many cases variance increases when using a higher order function. We select the simpler, linear function to represent the single-segment data. Similar linear scaling is proposed Hatton *et al.* (1994) for tensile fractures which (like veins observed in this study) are large compared to the grain scale of the fractured material.

Comparison of aspect ratios for single- and multi-segment data sets consistently shows larger aspect ratios for single-segment fractures than for the multi-segment fractures formed in the same lithology and tectonic environment. Single-segment veins have larger aspect ratios than their multi-segment counterparts (Figs. 3 and 5). Normalizing single- and multiple-segment fractures formed in the same environment supports this observation. Figure 9(a) shows two fractures from Culpeper Quarry with lengths normalized. The apertures are normalized to the lengths in order to preserve the relative aspect ratios. The same procedure is performed on two veins from Florence Lake (Fig. 9b). In both cases the aspect ratios for the single-segment fractures are an order of magnitude greater than those of multi-segment fractures.

Table 1. Single-segment data sets with average aspect ratios listed according to rock type and correlation coefficient

Location	Rock type	Vein filling	Aspect ratio	R^2
Forillon Park #2	Limestone	Calcite	7.3×10^{-3}	0.94
Forillon Park #1	Limestone	Calcite	8.2×10^{-3}	0.86
Ganister Quarry	Limestone	Calcite	2.5×10^{-3}	0.28
Bonticou Crag	Conglomerate	Quartz	3.1×10^{-3}	0.96
Culpeper Quarry	Siltstone	Calcite	3.4×10^{-3}	0.78
Anse a Mercier	Sandstone	Calcite	3.1×10^{-3}	0.76
Petite Vallee	Sandstone	Quartz	3.3×10^{-3}	0.68
Les Petit Anse	Sandstone	Calcite	4.4×10^{-3}	0.66
Lake Champlain	Argillite	Calcite	7.7×10^{-4}	0.22
Florence Lake	Granodiorite	Chlorite	1.9×10^{-3}	0.96
Whitehall Dike	Diabase	Calcite	1.5×10^{-3}	0.66

Data sets for multiple-segment fractures display greater scatter, smaller average aspect ratios (3.2×10^{-4} for Culpeper Quarry and 2.1×10^{-4} for Florence Lake) and are equally or marginally better fit by using a square root function as opposed to a linear function (Fig. 10). We interpret the multi-segment fractures using the Pollard *et al.* (1982) model for dilations of interacting crack arrays. Pollard *et al.* (1982) utilize a boundary element technique to develop numerical solutions for the elastic interactions of closely spaced cracks. Their generalized solution for an array of equal length segments (Pollard *et al.* 1982, fig. 16) is calculated numerically utilizing a regular, simplified geometry relating the segments. This geometry is defined using parameters that can be equated to our length, offset and overlap measurements. The parameter values they have used for this solution compare reasonably well with measurements made in this study.

We used values calculated by Pollard *et al.* (1982) for dilations of the central crack in each array as estimates of the maximum dilations for multi-segment fractures. To generalize the numerical results in a form compatible with our data presentation, we assume, consistent with

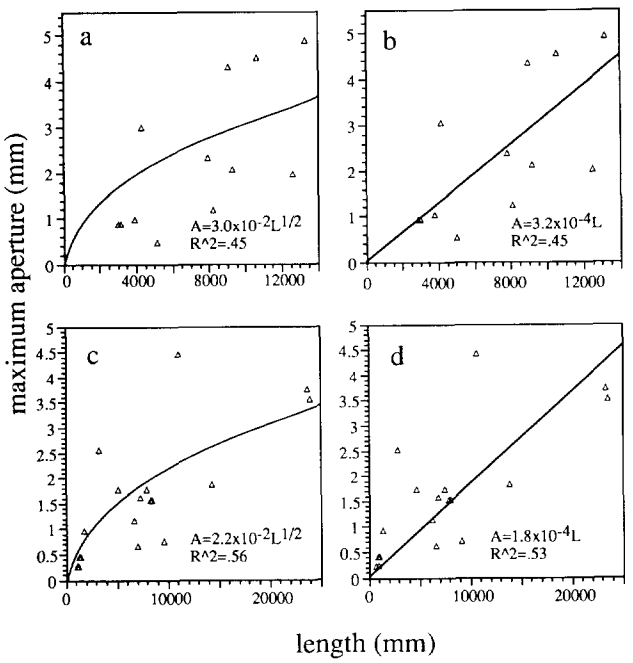

Fig. 10. Data for multiple-segment fractures from Culpeper Quarry (a) & (b) and Florence Lake (c) & (d). The square root function gives an equally good or marginally better fit for multi-segment fractures.

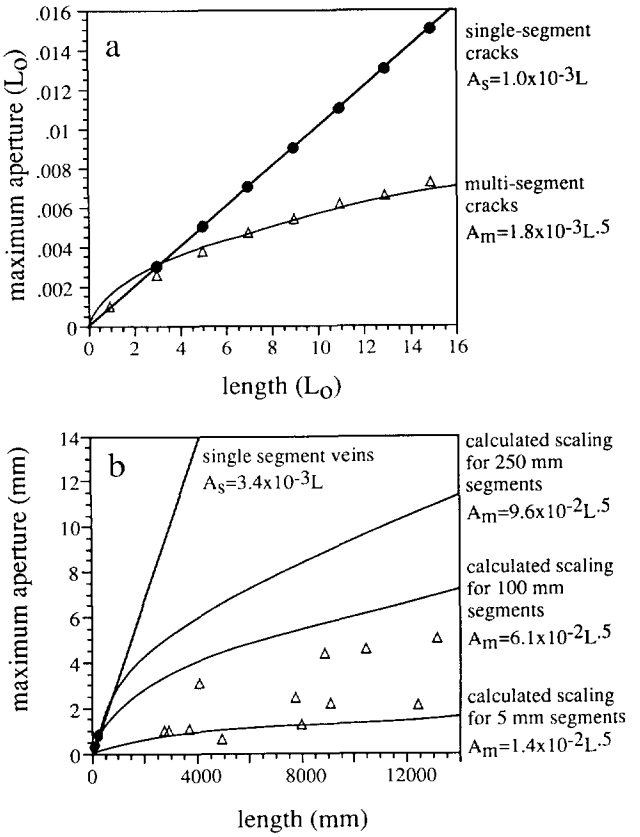

Fig. 11. Theoretical scaling for interacting elastic cracks (A_s = maximum aperture for single-segment fracture, A_m = maximum aperture for multi-segment fracture, L_o=idealized segment length, L = total fracture length). (a) Linear scaling for single segment cracks (●) and non-linear scaling for interacting non-connected segments, plotted in units of the segment length, L_o. The curved line represents a square root function fit to the numerical results (Δ) from Pollard *et al.* (1982). (b) Field data from Culpeper Quarry with linear scaling based on observations of single segment fractures (•) and non-linear scaling calculated for multi-segment fractures with segment lengths of 250 mm, 100 mm and 5 mm, along with observed data from multi-segment veins (Δ) (after Pollard *et al.* 1982).

our observations, that isolated cracks obey a linear aperture-length relationship:

$$A_s = C_1 L \tag{1}$$

where A_s is the maximum single-segment aperture and L is the length. For the example shown in Fig. 11(a) $C_1 = 1.0 \times 10^{-3}$, a geologically representative aspect ratio. We then assume that multiple-segment cracks consist of N segments of equal length (L_o), so that the total length,

$$L = NL_o \tag{2}$$

for such segmented cracks. Using the results from fig. 16 of Pollard *et al.* (1982) we calculate the maximum aperture, A_m, for the segmented crack. This result shows that for $N \geq 5$, the numerical results are well represented by the analytical expression

$$A_m = C_2 L^{.5}. \tag{3}$$

This expression is consistent with the nonlinear fits in Fig. 10. In the example shown $C_2 = 1.8 \times 10^{-3}$ (Fig. 11a). The constant C_2 is dependent on lithology and geologic environment (which are represented by the value of C_1), and is also dependent on the relative geometry and length of the segments making up the array. The constant for the multi-segment fractures can be expressed as:

$$C_2 = (C_1 L^{.5})/N + d/L^{.5} \tag{4}$$

where d is the additional dilation imposed by elastic interactions on the central segment of the array. There is no simple analytical solution for this additional dilation. Its magnitude varies with changes in length, offset and overlap of the segments.

Data for single-segment and multiple-segment fractures from Culpeper Quarry are plotted in Fig. 11(b). The linear function that results from fitting a line to the single-segment data gives a value for C_1. A value for C_2 is calculated using equation (4), this value of C_1 and d estimated from Pollard *et al.* (1982) model. Calculations based on L_o = 250 mm (median length of measured segments) predicts larger dilations than observed. While a histogram of segment lengths for this vein set shows a peak at 100–200 mm (Fig. 12) the data are better fit by calculations using segments ranging in length between 5 and 100 mm. We suggest that even individual segments form by the coalescence of smaller segments, and in a sense retain a memory of smaller component segments, due to incomplete connection. Abundant kinks along the length of multi-segment veins (as in Fig. 4c) support this suggestion. This model explains three features of our observations. First, segmented veins have smaller aspect ratios than single veins in the same vein set. Second, some vein segments have larger aspect ratios than single- or multi-segment veins within that set. Third, although aperture appears to scale linearly with length for single-segment veins, it appears to scale

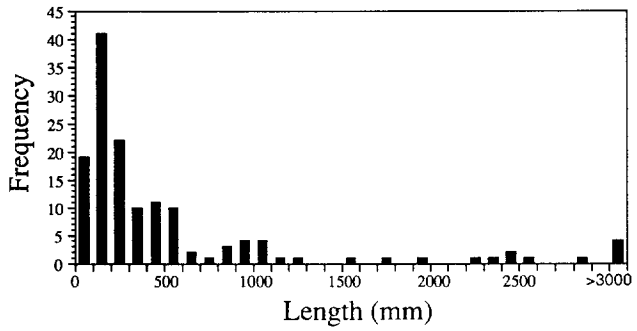

Fig. 12. Frequency-length plot for fracture segments in Culpeper Quarry.

nonlinearly for segmented veins, with an exponent of less than one.

We can consider the total amount of lateral offset between all segments with a fracture as a measure of the degree of connectedness of the segments. Fractures with greater total offset display smaller aspect ratios than comparable fractures with smaller total offset. This is seen in Fig. 13, in which two multi-segment veins from Culpeper Quarry display different degrees of connectedness. The 32-segment vein in Fig. 13(a) is made up of non-connected to partially connected segments, with a total perpendicular offset of 4.5% of the total vein length. The 15 segments in Fig. 13(b) are all well connected, looking like Fig. 4(c). The total offset is only 1.4% of the length. The aspect ratio for the well-connected vein is significantly larger than the aspect ratio for the less well-connected vein. The variability of connectedness for multiple-segment fractures contributes to scatter in the data sets.

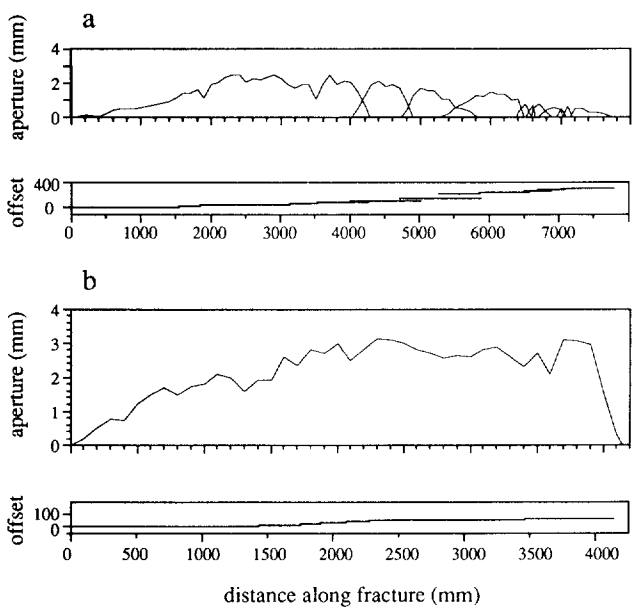

Fig. 13. Displacement-length plots and segment offset maps for two fractures from Culpeper Quarry. (a) Fracture composed of non-connected to partially connected segments, total offset = 351.7 mm = 4.5%L. $A/L = 3.1\times10^{-4}$. (b) Fracture composed of well-connected segments, total offset = 55.9 mm = 1.4%L. $A/L = 7.5 \times 10^{-4}$.

DISCUSSION

Single-segment fractures

The geometries observed in displacement-length profiles show centrally located maxima and tapered displacement gradients at the tips, consistent with Dugdale's (1960) elastic-plastic model. The tapered tips represent zones of inelastic deformation (of length s), where stresses cannot exceed the tensile yield strength (σ_y) of the material. Values for s were measured on displacement profiles in which there were distinct inflection points along the profile. The length of s is not discernable on all fractures, but the s/L ratio is relatively constant for each data set.

The Dugdale model predicts the observed linear scaling between maximum aperture (A_{max}) and length (L) in which the constant of proportionality represents a ratio between the yield strength and shear modulus (μ) for the fractured lithology. The value for this constant is given by:

$$\frac{A_{max}}{L} = \frac{(1-\nu)\sigma_y}{2\pi\mu}\left[\cos\theta_2 \log_e \frac{(\sin\theta_2 + 1)^2}{(\sin\theta_2 - 1)^2}\right], \quad (5)$$

in which ν is Poisson's ratio. The trigonometric term inside the bracket is the solution to the elastic problem by the method of Muskhelishvili (1954) in which:

$$\cos\theta_2 = \frac{(L-2s)}{L} \quad (6)$$

(Cowie & Scholz 1992). The tensile yield strength can be estimated utilizing equation (5), observed vein geometries and reasonable estimates of elastic moduli. The yield stress for the formation of the veins near Florence Lake was estimated using the average aspect ratio for single-segment veins of 1.9×10^{-3}, $s/L = 0.11$ and moduli values for Raymond granodiorite from laboratory and *in situ* measurements (Pratt *et al.* 1972). Since their laboratory determinations for μ exceed their *in situ* values by nearly a factor of two, we have used minimum and maximum values of $\mu = 1.1 \times 10^4$ MPa and 2.2×10^4 MPa. Estimates of minimum and maximum values for yield stress are 74 MPa and 148 MPa. The yield stress represents the tensile strength of the material. This critical stress need only be attained locally, at the crack tip for fracture propagation. The magnitude of the driving stress (σ_d = the difference between the fluid pressure within the crack and the remote normal stress) required for fracture formation is given by:

$$\sigma_d = \frac{4\sigma_y}{\pi}\sin^{-1}\sqrt{\frac{s}{L}} \quad (7)$$

(Dugdale 1960). Driving stresses calculated for the Florence Lake fractures are 32–63 MPa. These values are comparable to driving stresses calculated using a simple elastic model in which:

$$\sigma_d = \frac{A_{max}\mu}{L(1-\nu)} \quad (8)$$

(Pollard & Segall 1987). Using the same values for elastic moduli and equation (8) estimates of the driving stress are 27–46 MPa. Laboratory derived values for the tensile strength of granitic rocks range from a few to several tens of MPa (Lama & Vutukuri 1978). Our computed stress values are consistent with the high end of this range.

Similar calculations for the veins in Culpeper Quarry using $A_{max}/L = 3.4 \times 10^{-3}$, $s/L = 0.07$ and moduli values from Miller (1965) of $\nu = 0.22$ and $\mu = 5.5 \times 10^3$ MPa and 1.1×10^4 MPa, give yield stresses between 78 and 156 MPa and driving stresses of 27–54 MPa. These values are consistent with the high end of the range of laboratory derived tensile strengths for siltstone of a few to a few tens of MPa (Lama & Vutukuri 1978).

The driving stresses computed in this study are at the high end of the large range of measured earthquake stress drops of 0.03–30 MPa (Hanks 1977) and are consistent with *in situ* minimum horizontal stress measurements of 2–80 MPa (Haimson & Voight 1977, Zoback *et al.* 1977) for hydrofracture at depths to a few hundred meters. Gudmundsson (1983) estimates the depth of formation (D) for dikes by utilizing dike geometry to calculate values for the driving stress. With assumed densities for the fractured rock (ρ_r) and the magma (ρ_m) depth is calculated with the equation:

$$D = \frac{\sigma_d}{(\rho_r - \rho_m)g} \tag{9}$$

where g is the acceleration due to gravity. Using this equation the depth of formation for the veins near Florence Lake is estimated to be 2–4 km using a density of 2700 kgm^{-3} for granodiorite (Turcotte & Schubert 1982) and $\rho_m = 1000$ kgm^{-3} for hydrous fracture-filling fluid. Using a density of 2300 kgm^{-3} for siltstone (Leavy *et al.* 1983) a formation depth of 2–3 km is calculated for the veins in Culpeper Quarry.

While the stresses and depths calculated seem geologically reasonable lack of good constraints on the elastic moduli at depth and uncertainty in values for s prohibit resolution. The Dugdale (1960) model is limited to two dimensions. Since deformation is not restricted to a plane but takes place within a volume of rock surrounding the crack tip, values for the parameter s are sometimes poorly defined.

Multiple-segment fractures

The segmentation of longer fractures suggests that they have developed by the coalescence of smaller fractures. Formation of en échelon segments has been modeled as the breakdown of a larger parent crack (e.g. Pollard *et al.* 1982). Lack of observation of non-segmented parent cracks makes this interpretation inconsistent with our data. Smaller aspect ratios for multi-segment fractures suggests that when two segments join, the connection is incomplete, even for apparently well-connected fracture segments. Slight variations in strike and dip along with lateral offsets, impede the dilation of the connected segments.

Elastic theory has been used successfully to describe alterations of the stress and deformation fields near the tip of a mode I crack (Lawn & Wilshaw 1975, Delaney & Pollard, 1981). Pollard *et al.* (1982) use these localized stress and displacement changes to describe the interaction of deformation fields for closely spaced cracks. Their theoretical results predict two of the observations made in this study. First, there is a reduction in aperture for multiple-segment crack arrays when compared to single-segment cracks of the same length. Second, individual segments within a multi-segment array have higher aspect ratios than isolated cracks of the same length. Variations in the geometry, size and number of segments making up multiple segment fractures result in a range of aspect ratios for fractures of any given length. Aperture is in general a non-linear function of total length for segmented veins. As in the case of single-segment veins the displacement profiles for multi-segment veins have a shape more consistent with Dugdale's (1960) elastic-plastic model than a purely elastic model. This is not entirely inconsistent with our interpretation of these veins using an elastic interaction model because the elastic-plastic model implies that plastic yielding is restricted to the immediate vicinity of the segment tips. The longer range interaction stresses are still elastic in such a model.

Comparison with faults

Many of the observations made in this study of extension fractures are similar to observations made in recent studies involving faults. Cowie & Scholz (1992) used Dugdale's (1960) work as the basis for a fault growth model, which predicts linear scaling between shear displacement and length, with the constant of proportionality dependent on the ratio of the shear strength to the shear modulus of the faulted rock. Aspect ratios for faults of 1.2×10^{-2} (Muraoka & Kamata 1983), 1.2×10^{-2} (Opheim & Gudmundsson 1989), 2.9×10^{-2} (Villemin *et al.* in press), 3.6×10^{-3} (Peacock & Sanderson 1991) and 1.0×10^{-2} (Dawers *et al.* 1993) are consistent with shear strengths roughly an order of magnitude greater than tensional strengths implied by the aspect ratios for veins reported here.

Some faults, like fractures, are composed of multiple segments. Displacement-length profiles for multiple-segment faults or fault zones display coherent profiles with displacement deficits at segment offsets (Peacock & Sanderson 1991). In both normal and strike slip faults, the average aspect ratio for individual segments within multi-segment faults are larger than aspect ratios for the fault zone as a whole. The average aspect ratio for normal fault segments measured by Peacock & Sanderson (1991) is 7.7×10^{-3} as compared with 3.6×10^{-3} for the fault zone as a whole. Peacock (1991) reports an average aspect ratio of 2.1×10^{-2} for strike slip fault segments while the aspect ratios for two of the fault zones containing these segments are 6.3×10^{-3} and 9.3×10^{-3}.

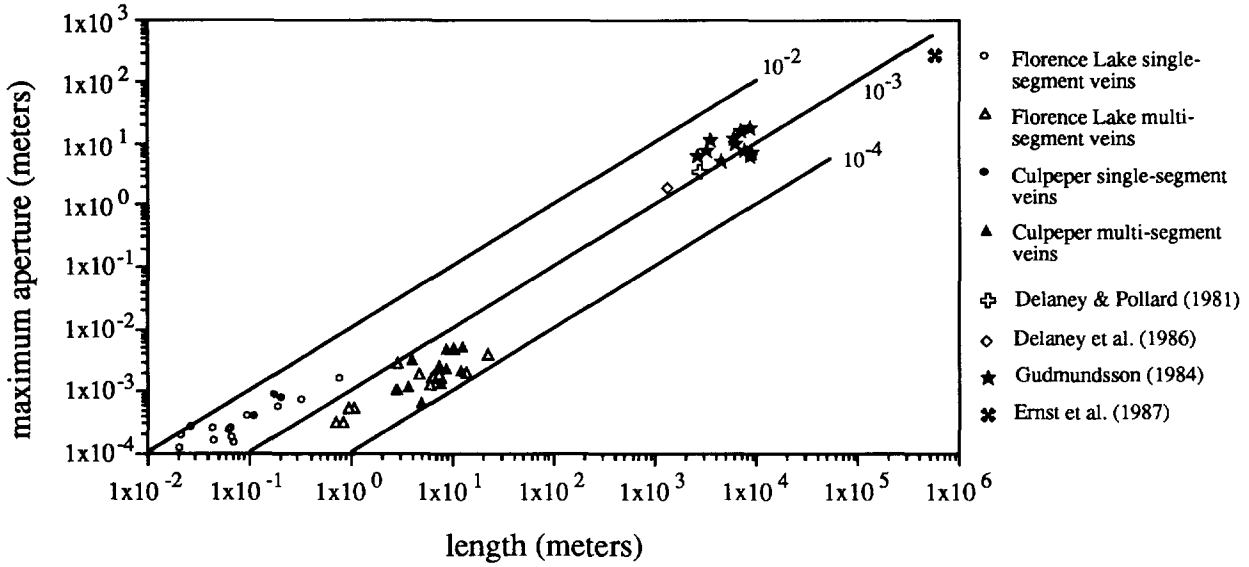

Fig. 14. Logarithmic plot of fracture length against fracture aperture for Florence Lake, Culpeper Quarry and published data for mafic dikes.

Data from mafic dikes

The fractures measured in this study range in length from 7 mm to 23.7 m, covering three orders of magnitude. This range can be extended to six orders of magnitude with the addition of data from the literature on extensional mafic dikes. In Fig. 14 the data from Florence Lake and Culpeper Quarry are plotted along with dike data. The 600 km long Great Abitibi Dyke in Canada is one of the longest in the world (Ernst *et al.* 1987). Basaltic dikes in Iceland (Gudmundsson 1984) are tens of km long. Delaney & Pollard (1981) and Delaney *et al.* (1986) measured mafic dikes about 1 km long, on the Colorado Plateau in the southwestern U.S.A.

Mafic dikes have been modeled utilizing the principles of fracture mechanics applied to mode I cracks (Delaney & Pollard 1981, Pollard *et al.* 1983, Pollard 1987, Pollard & Segall 1987). While differences in fracture filling materials (magma in dikes as opposed to hydrothermal deposits in veins), possibilities of pressure gradients within dikes and evidence for incremental growth in some dikes give cause for concern, the similarities in the geometry of veins and dikes supports the combination of these data. The data help to define a linear scaling relationship between length and maximum aperture. The constant of proportionality varies for each data set, depending on the lithology and tectonic environment. Segmentation of longer fractures within each data set results in a break in scaling between single- and multi-segment fractures. The multiple-segment fractures plot in clusters falling between lines representing two end-member models. The linear trend of the single-segment fractures defining the upper boundary, represents perfectly connected segments. At the lower boundary, aperture scales with the square root of length, modeling the fracture segments as non-connected but interacting en échelon fracture segments.

CONCLUSIONS

Fractures observed at all seven field locations display displacement profiles with centrally located maxima and gentle displacement gradients at the tips. This shape, present in both single- and multiple-segment fractures, is consistent with elastic-plastic models for fracture growth.

Displacement profiles for multiple-segment fractures can be used to examine the connectedness of the segments. Coherent profiles provide support for considering closely spaced, sub-parallel segments as a single unit when computing aperture-length ratios. The aspect ratios of individual segments and subunits of associated segments within multi-segment fractures, also provide evidence that these segments are not isolated features, but dependent parts of larger fractures. Aspect ratios for single-segment fractures are consistently larger than aspect ratios for multi-segment fractures formed in the same rock type and tectonic environment.

Maximum displacement-length plots indicate a linear relationship between length and aperture for single-segment fractures. These fractures plot in clusters along linear trends for separate data sets. There is a break in scaling between single- and multiple-segment fractures for each field location. Multiple-segment fractures plot in clusters falling between lines representing the linear trend of the single-segment fractures and a square root function representing the fracture segments as non-connected but interacting en échelon fracture segments. Aspect ratios for veins and mafic dikes fall between 2.1 $\times 10^{-4}$ and 8.2 $\times 10^{-3}$. These aspect ratios are consistent with tensile strengths an order of magnitude lower than shear strengths implied by aspect ratios for displacements on faults.

Acknowledgements—The authors would like to thank Ed Beutner, Terry Engelder, Robert Hatcher, Chris Barton and Paul Segall for suggestions regarding field locations. Nick Christi-Blick, Mark

Anders, Paul Delaney and Steve Laubach provided helpful reviews of the manuscript. This project was generously supported by Lawrence Livermore National Laboratory contract #LLNL B157348. Lamont contribution # 5252.

REFERENCES

Barton, C. A. & Larsen, E. 1985. Fractal geometry of two-dimensional fracture networks at Yucca Mountain, southwestern Nevada. In: *Proceedings of the International Symposium on Fundamentals of Rock Joints*. Bjorkliden, Sweden, 77–84.

Broek, D. 1974. *Elementary Engineering Fracture Mechanics*. Noordhoff, Leyden.

Bürgmann, R., Pollard, D. D. & Martel, S. J. 1994. Slip distributions on faults: effects of stress gradients, inelastic deformation, heterogeneous host-rock stiffness and fault interaction. *J. Struct. Geol.* **16**, 1675–1690.

Cowie, P. A. & Scholz, C. H. 1992. Physical explanation for displacement-length relationship of faults using a post-yield fracture mechanics model. *J. Struct. Geol.* **14**, 1133–1148.

Dawers, N. H., Anders, M. H. & Scholz, C. H. 1993. Growth of normal faults: displacement-length scaling. *Geology* **21**, 1107–1110.

Delaney, P. T. & Pollard, D. D. 1981. Deformation of host rocks and flow of magma during growth of minette dikes and breccia-bearing intrusions near Ship Rock, New Mexico. *U.S. Geol. Sur. Prof. Pap.* **1202**, 1–61.

Delaney, P. T., Pollard, D. D., Ziony, J. I. & McKee, E. H. 1986. Field relations between dikes and joints: emplacement processes and paleostress analysis. *J. geophys. Res.* **91**, 4920–4938.

Dugdale, D. S. 1960. Yielding of steel sheets containing slits. *J. Mech. Phys. Solids* **8**, 100–104.

Epstein, J. B. & Lyttle, P. T. 1987. Structure and stratigraphy above, below, and within the Taconic unconformity, southeastern New York. In: *New York State Geol. Assoc. 59th Ann. Mtg. Kingston, N.Y. Nov. 6–8, 1987 Field Trip Guidebook* (edited by Waines, R. H.). New Paltz, N.Y. State Univ. New York, C1–C78.

Ernst, R. E., Bell, K., Ranalli, G. & Halls, H. C. 1987. The great Abibiti Dyke, southeastern Superior Province, Canada. In: *Mafic Dyke Swarms* (edited by Halls, H. C. & Fahrig, W. F.). *Spec. Pap. geol. Ass. Can.* **34**, 123–135.

Fisher, D. W. 1968. Geology of the Plattsburgh and Rouses Point, New York–Vermont, Quadrangles. *New York State Museum Map and Chart Series* **10**, 1–51.

Fisher, D. W. 1984. Bedrock geology of the Glens Falls-Whitehall region, New York. *New York State Museum Map and Chart Series* **35**, 1–58.

Geiser, P. A. & Engelder, T. 1983. The distribution of layer parallel shortening fabrics in the Appalachian foreland of New York and Pennsylvania: Evidence for two non-coaxial phases of the Alleghian orogeny. *Mem. geol. Soc. Am.* **158**, 161–175.

Goodier, J. N. & Field, F. A. 1963. Plastic energy dissipation in crack propagation. In: *Fracture of Solids* (edited by Drucker, D. C. & Gilman, J. J.). Wiley, New York. 103–118.

Gudmundsson, A. 1983. Form and dimensions of dykes in eastern Iceland. *Tectonophysics* **95**, 295–307.

Gudmundsson, A. 1984. Tectonic aspects of dykes in northwestern Iceland. *Jokull* **34**, 81–96.

Haimson, B. C. & Voight, B. 1977. Crustal stress in Iceland. *Pure & Appl. Geophys.* **115**, 153–190.

Hanks, T. C. 1977. Earthquake stress drops, ambient tectonic stresses and stresses that drive plate motions. *Pure & Appl. Geophys.* **115**, 441–458.

Hatton, C. G., Main, I. G. & Meredith, P. G. 1994. Non-universal scaling of fracture length and opening displacement. *Nature* **367**, 160–162.

Lama, R. D. & Vutukuri, V. S. 1978. *Handbook on Mechanical Properties of Rock: Testing Techniques and Results*. Series on Rock and Soil Mechanics II, Trans Tech Clausthal.

Lawn, B. R. & Wilshaw, T. R. 1975. *Fracture of Brittle Solids*. Cambridge University Press, Cambridge.

Leavy, B. D., Froelich, A. J. & Abram, E. C. 1983. Bedrock map and geotechnical properties of rocks of the Culpeper Basin and vicinity, Virginia and Maryland. *Misc. Inv. Series of U.S. Geol. Sur.*, I-1313-C, 1:125,000.

Miller, R. P. 1965. Engineering classification and index properties for intact rock. Ph.D. Thesis, Univ. Ill., Urbana, Ill.

Muraoka, H. & Kamata, H. 1983. Displacement distribution along minor fault traces. *J. Struct. Geol.* **5**, 483–495.

Muskhelishvili, N. I. 1954. *Some Basic Problems of the Mathematical Theory of Elasticity* (translated by Radok, J. R. M.). Noordhoff, Leyden.

Olsen, P. E. & Schlische, R. W. 1989. Tectonic history. In: *Tectonic, Depositional, and Paleocological History of Early Mesozoic Rift Basins, Eastern North America* (edited by Olsen, P. E., Schlische, R. W. & Gore, P. J. W.). Field trip guide book T351, *Am. Geophys. U.* 12–14.

Opheim, J. A. & Gudmundsson, A. 1989. Formation and geometry of fractures, and related volcanism, of the Krafla fissure swarm, northeast Iceland. *Bull. geol. Soc. Am.* **101**, 1608–1622.

Peacock, D. C. P. 1991. Displacements and segment linkage in strike-slip fault zones. *J. Struct. Geol.* **13**, 1025–1035.

Peacock, D. C. P. & Sanderson, D. J. 1991. Displacements, segment linkage and relay ramps in normal fault zones. *J. Struct. Geol.* **13**, 721–733.

Pollard, D. D. 1987. Elementary fracture mechanics applied to the structural interpretation of dykes. In: *Mafic Dyke Swarms* (edited by Halls, H. C. & Fahrig, W. F.). *Spec. Pap. geol. Ass. Can.* **34**, 123–135.

Pollard, D. D. & Aydin, A. 1988. Progress in understanding jointing over the past century. *Bull. geol. Soc. Am.* **100**, 1181–1204.

Pollard, D. D., Delaney, P. T., Duffield, W. A., Endo, E. T. & Okamura, A. T. 1983. Surface deformation in volcanic rift zones. *Tectonophysics* **94**, 541–584.

Pollard, D. D. & Segall, P. 1987. Theoretical displacements and stresses near fractures in rock: with applications to faults, joints, veins, dikes, and solution surfaces. In: *Fracture Mechanics of Rock* (edited by Atkinson, B.). Academic Press, London.

Pollard, D. D., Segall, P. & Delaney, P. T. 1982. Formation and interpretation of dilatant echelon cracks. *Bull. geol. Soc. Am.* **93**, 1291–1303.

Pratt, H. R., Black, A. D., Brown, W. S. & Brace, W. F. 1972. The effect of specimen size on the mechanical properties of unjointed diorite. *Int. J. Rock Mech. & Min. Sci.* **9**, 513–529.

Press, W. H., Flannery, B. P., Teukolsky, S. A. & Vetterling, W. T. 1986. *Numerical Recipes: The Art of Computing*. Cambridge University Press, London.

Ramsay, J. G. 1980. The crack-seal mechanism of rock deformation. *Nature* **284**, 135–139.

Scholz, C. H. & Cowie, P. A. 1990. Determination of total strain from faulting using slip measurements. *Nature* **346**, 837–839.

Segall, P. & Pollard, D. D. 1983. Joint formation in granitic rock of the Sierra Nevada. *Bull. geol. Soc. Am.* **94**, 563–575.

Srivastava, D. C. & Engelder, T. 1991. Fluid evolution history of brittle-ductile shear zones on the hanging wall of Yellow Spring Thrust, Valley and Ridge Province, Pennsylvania, U.S.A. *Tectonophysics* **198**, 23–34.

Turcotte, D. L. & Schubert, G. 1982. *Geodynamics: Applications of Continuum Physics to Geological Problems*. Wiley, New York.

Villemin, T., Angelier, J. & Sunwoo, C. In press. Fractal distribution of fault lengths and offsets: implications for brittle deformation evaluation: The Lorraine Coal Basin (NE France). In: *Fractals and Their Use in the Petroleum Industry* (edited by Barton, C. & LaPointe, P.). *Am. Ass. Petrol. Geol.* Book Series.

Zoback, M. D., Healy, J. H. & Roller, J. C. 1977. Preliminary stress measurements in central California using the hydraulic fracturing technique. *Pure & Appl. Geophys.* **115**, 135–152.

APPENDIX: FIELD LOCATIONS

Bonticou Crag

Quartz-filled fractures cutting the Shawangunk Formation were measured on Bonticou Crag, 5.3 km north-northwest of New Paltz, New York. The Shawangunk Formation is an orthoquartzite-pebble conglomerate of Middle Silurian age (Epstein & Lyttle 1987). Offsets of fractured pebbles indicate extensional displacements for these single-segment veins. The N–NW strike of the veins is consistent with an early Alleghenian phase of north-northwest oriented compression suggested by Geiser & Engelder (1983). Microscopic examination of vein material shows blocky quartz in optical continuity with wallrock grains.

Gaspe Peninsula

Calcite- and quartz-filled fractures cutting limestones and sandstones were measured on the Gaspe Peninsula, Quebec, Canada. Measurements were made at five locations. Calcite extension fractures cut Lower Devonian limestones near Cap-Bon-Ami in Forillon National Park. Veins were measured in beds of the Cap-Bon-Ami Formation, 3 km north of Cap-Bon-Ami and on Quay Rock. Calcite-filled fractures in calcareous sandstones of the Middle Ordovician Cloridorme Formation were measured along the coast at Anse a Mercier and Les Petite Anse, both west of Grande-Vallee. Quartz veins in sandstones of the same formation were measured at Petite-Vallee. The orientations of the 56 fractures measured on the Gaspe Peninsula are normal to Paleozoic fold axes. Microscopic examination of the vein-filling material shows grains nucleating along the fractured wall rock grains with elongated axes extending toward the vein centers.

Whitehall Dike

Mineralized fractures were measured on the horizontal, glacially polished surface of a Proterozoic diabase dike, 1 km east of Whitehall, New York (Fisher 1984). These steeply dipping calcite veins do not affect the surrounding country rock but are restricted to the intrusion and may represent cooling features. Microscopic examination reveals chlorite grains oriented parallel to the vein walls within the calcite vein material. This structure is not visible in the field and is obscured on the microscopic scale by chlorite alteration. This structure may indicate crack-seal growth of the veins or shear deformation, either of which could result in altered geometry for these veins.

Lake Champlain

Horizontal beds of Upper Ordovician Cumberland Head Argillite and overlying Stony Point Shale are found in wave-polished outcrops along the west shore of Lake Champlain, 5 km east of Plattsburgh, New York and on South Hero Island, Vermont. A system of vertical, N-striking calcite veins cuts both formations. Although the veins in this set consistently offset the first and most dominant cleavage in the rocks, they are offset by a later, less well developed widely spaced pressure solution cleavage, indicating syntectonic formation. The tectonic history of the Champlain Valley is complex and the significance of this fracture set's orientation in relation to other tectonic structures is not clear (Fisher 1968). Vein traces on step-like, bedding-perpendicular exposures display larger aspect ratios than the dominant bedding-parallel exposures. This outcrop geometry while providing information on the three dimensional shape of the fractures, provides incomplete exposure of bedding plane surfaces. It is possible that apparently isolated fractures measured on these surfaces may actually be segments from unexposed multiple-segment arrays. Large scatter for single segment veins from this location may result from this measurement error. Thin sections show blocky calcite vein fill.

Ganister Quarry

An outcrop of Upper Ordovician carbonates in Ganister Quarry (2.3 km northwest of Williamsburg, Pennsylvania) contains calcite, dolomite and quartz filled mode I fractures, in exposures of Coburn Formation limestone. Data were collected for all veins intersecting an 80 m^2 exposure of a bedding plane (Fig. 2a). Some veins showed evidence of shear deformation and/or crack-seal morphology (Ramsay 1980) indicating several incremental growth events. Therefore, a subset of undeformed, single-event fractures was selected, by visual inspection, from the larger data set (Fig. 2b). The formation of this NW-oriented, bedding-perpendicular, calcite-filled vein set is consistent with strike-parallel stretching of beds during Appalachian thrusting (Srivastava & Engelder 1991). Microscopic inspection of veins from the selected subset show equant calcite grains.

Culpeper Quarry

The recent discovery of multiple sets of dinosaur footprints on a single bedding plane in Culpeper Crushed Stone Quarry (Stevensburg, Virginia) resulted in excavation and preservation of a 70,000 m^2 surface. This excellent bedding plane exposure of calcareously cemented Balls Bluff Siltstone (Upper Triassic, from the Bull Run Formation of the Culpeper Group), contains several vein sets. Lithologic markers cut by a NE-trending, bedding plane-perpendicular set of calcite-filled fractures indicate extensional displacement. The orientation of this vein set is compatible with the northwest extension direction postulated for the formation of Culpeper and associated early Mesozoic rift basins (Olsen & Schlische 1989).

The fine grained nature of the rock and sharp contrast between the dark-red siltstone and the white calcite vein filling make detailed measurement of fine segment terminations possible. For this reason Culpeper Quarry was selected for a detailed study of segmentation. Thin-sections of single segment veins display blocky calcite grains. One multi-segment vein shows trails of wall-rock inclusions parallel to vein walls in ordinary and polarized light. Cathodoluminescence reveals a layered structure within the vein. These structures indicate crack-seal growth, resulting in exaggerated aspect ratios.

Florence Lake

Florence Lake is located in the central Sierra Nevada about 90 km northeast of Fresno, California. Spectacular exposures of glacially polished Mount Givens Granodiorite are cut by a N–NE striking set of steeply dipping chlorite- and epidote-filled fractures (Segall & Pollard 1983). Larger veins are enclosed in zones of altered granodiorite. These zones are more resistant to erosion than the surrounding wall rock, forming conspicuous raised ridges. Offsets on mineral grains and pre-existing aplite dikes show extensional displacements normal to the vein walls. Longer veins are composed of multiple sets of closely-spaced segments. In small exposures perpendicular to the major outcrop surfaces, some separate segments can be seen to be connected at depth. Measurement of fine vein details was aided by the low water level in Florence Lake which exposed a band several to tens of meters wide that was free from lichen. Microscopic inspection of the vein fill shows randomly oriented chlorite and epidote grains.